AFFTC-PA-11253

COMPRESSOR MODELING FOR ENGINE CONTROL AND MAINTENANCE

CAPT CARL BECKEY, USAF
DR. ROY HARTFIELD
DR. MARK CARPENTER

AIR FORCE FLIGHT TEST CENTER
EDWARDS AFB, CA

JULY 2011

AIR FORCE FLIGHT TEST CENTER
EDWARDS AIR FORCE BASE, CALIFORNIA
AIR FORCE MATERIEL COMMAND
UNITED STATES AIR FORCE

AFFTC

REPORT DOCUMENTATION PAGE

Form Approved
OMB No. 0704-0188

1. REPORT DATE *(DD-MM-YYYY)*	**2. REPORT TYPE**	**3. DATES COVERED** *(From - To)*
18-07-2011		07-06-2007 – 19-09-2010

4. TITLE AND SUBTITLE
Compressor Modeling for Engine Control and Maintenance

5a. CONTRACT NUMBER

5b. GRANT NUMBER

5c. PROGRAM ELEMENT NUMBER

6. AUTHOR(S)
Capt Carl Beckey, USAF
Dr. Roy Hartfield
Dr. Mark Carpenter

5d. PROJECT NUMBER

5e. TASK NUMBER

5f. WORK UNIT NUMBER

7. PERFORMING ORGANIZATION NAME(S) AND ADDRESS(ES) AND ADDRESS(ES)

418 FLTS,412 Test Wing, AFFTC
Edwards AFB CA 93524

8. PERFORMING ORGANIZATION REPORT NUMBER
AFFTC-PA-11253

9. SPONSORING / MONITORING AGENCY NAME(S) AND ADDRESS(ES)

418 FLTS, 412 Test Wing, AFFTC
Edwards AFB CA 93524

10. SPONSOR/MONITOR'S ACRONYM(S)
N/A

11. SPONSOR/MONITOR'S REPORT NUMBER(S)

12. DISTRIBUTION / AVAILABILITY STATEMENT
Approved for public release A: distribution is unlimited.

13. SUPPLEMENTARY NOTES
CA: Air Force Flight Test Center Edwards AFB CA CC: 012100

14. ABSTRACT
This work describes a method for dynamically updating the compressor map for an advanced turbofan engine. The implementation of the method is illustrated using data from a transport aircraft powered by four turbofan engines. The compressor map is generated through projection pursuit regression and non-linear approximation, using Bernstein polynomial basis expansion regression. This approach allows for prediction options which would be useful to a controller algorithm. Results include the compressor maps and recommendations for implementing the proposed approach in an engine management system.

15. SUBJECT TERMS

16. SECURITY CLASSIFICATION OF:			**17. LIMITATION OF ABSTRACT**	**18. NUMBER OF PAGES**	**19a. NAME OF RESPONSIBLE PERSON**
Unclassified					412 TENG/EN (Tech Pubs)
a. REPORT	**b. ABSTRACT**	**c. THIS PAGE**			**19b. TELEPHONE NUMBER** *(include area code)*
Unclassified	Unclassified	Unclassified	None	18	661-277-8615

Compressor Modeling for Engine Control and Maintenance

Carl Beckey,[1] Roy Hartfield,[2] Mark Carpenter[3]
Auburn University, Auburn, AL

Abstract

This work describes a method for dynamically updating the compressor map for an advanced turbofan engine. The implementation of the method is illustrated using data from a transport aircraft powered by four turbofan engines. The compressor map is generated through projection pursuit regression and non-linear approximation, using Bernstein polynomial basis expansion regression. This approach allows for prediction options which would be useful to a controller algorithm. Results include the compressor maps and recommendations for implementing the proposed approach in an engine management system.

Introduction

The refined turbofan engine offers unmatched performance and efficiency for heavy lift transport applications. This paper focuses on further refinements to the operation of the compressor. As air is ingested by the compressor, it travels through a complex array of rotating and stationary airfoils, pressure bleed valves and ducting. To analyze this flow and its effects on engine performance, real-world data has been captured from a turbofan engine and a parametric model of the operating conditions has been developed. The data captured during a range of operations has been used to develop a compressor map. Purely mathematically surrogate approaches to modeling compressor performance have been developed[1], however, in this case a parameterized modeling approach is used because of the higher likelihood of capturing some of the physics of the compressor performance with the model. This data has been reduced using Bernstein polynomials to generate a set of speed lines and a complete response surface for the compressor. This approach can be implemented dynamically to provide a continuously updated performance map available to the engine controller across the entire operating range for the engine. As components wear and deteriorate throughout the life of the engine, operating conditions can be adapted by the dynamic updating of the compressor map response surface. This provides full utilization of the operating envelope from the time an engine is placed on wing until it is removed, allowing for maximum efficiency, performance, and safety.

---

[1]Capt USAF
[2]Woltosz Professor, Department of Aerospace Engineering, Associate Fellow AIAA
[3] Professor, Department of Mathematics and Statistics, Member AIAA

Experimental Procedures

Data captured from each of the four engines of a heavy transport aircraft were used to conduct this analysis. This family of engines has a 6:1 bypass ratio and a maximum overall pressure ratio of just over 30. As seen in Figure 1, compression is provided by a dual spool compressor. The low pressure compressor (LPC) consists of a fan and four compressor stages, while the high pressure compressor (HPC) consists of a set of variable pitch inlet guide vanes (IGVs) and 12 compressor stages, of which the first four have variable pitch stators. Bleed air is pulled off four stages throughout the compressor to support a number of systems including aircraft pressurization, air-conditioning, anti-ice, inert gas generation, active clearance control and engine stability. Data is captured at a number of locations throughout the engine and combined with general aircraft operating conditions to provide detailed performance feedback. In the development of the analytical model, total pressure in pounds per square inch from stations 2, 3 and 4.9, total temperature in degrees Celsius from stations 2 and 4.9, weight of fuel flow in pounds per hour and RPM as a percent of maximum for the HPC and LPC have been utilized. The data has been recorded from multiple aircraft over a period of several days, during which time over ten thousand data points were captured. The data points include aircraft operation at a number of different airfields and conditions both in the United States and abroad. Furthermore, the data points cover a range of operating conditions, including climb, cruise, descent, landing, air-to-air refueling, low-level flight, high speed descents and multiple different airdrop profiles.

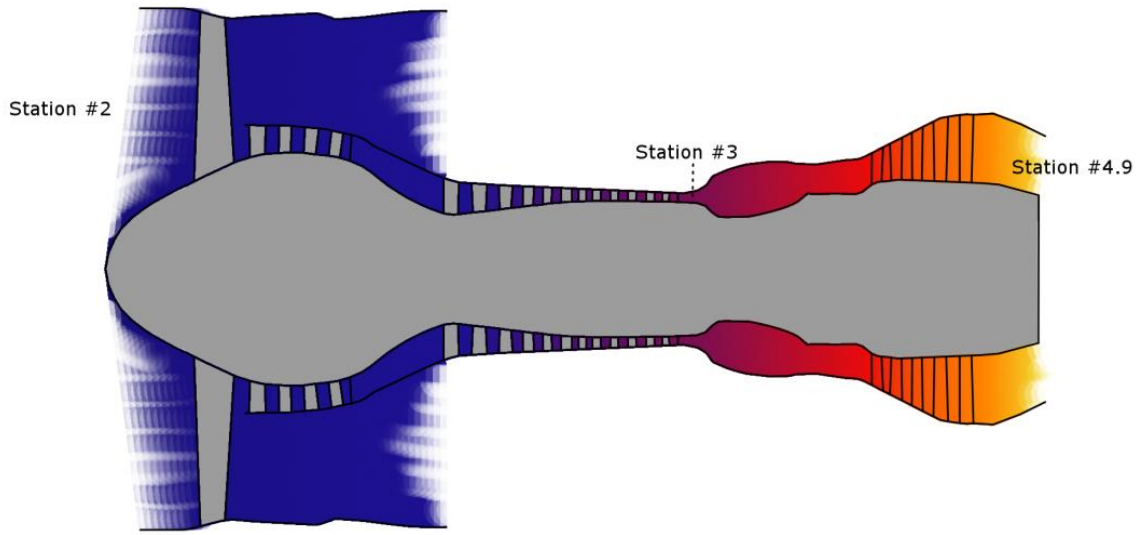

Figure 1: Turbofan station numbering diagram.

Data Reduction

The measurements as outlined above have been utilized to generate a compressor map and response surface for the compressor operation. In order to do so, it was necessary to first calculate the mass flow rate through the core of the engine. For this calculation, the conditions just downstream of the turbine were utilized. At this location, the total pressure was cross-referenced to the inlet conditions to check for choked flow conditions, as such the local velocity was assumed to be sonic. As a result, all data points where the pressure ratio was less than unity were rejected. Furthermore, to improve response accuracy, all data at and below ground idle RPM, were rejected. The remaining data was further reduced as follows. The total temperature aft of the turbine was utilized to calculate the local ratio of specific heats, which allows for the calculation of the mass flow parameter. For this calculation, the specific heat at constant pressure was first found using Equation 1.[2]

$$C_p = 0.2269807e^{0.000097247*T_t} \tag{1}$$

The ratio of specific heats is then given by Equation 2.

$$\gamma = \frac{C_p}{C_p - R} \tag{2}$$

The mass flow parameter is then calculated for the point just downstream of the turbine where the flow is assumed to be sonic, Mach equal to one. Given the ratio of specific heats and the Mach number, the mass flow parameter is given by Equation 3.[3]

$$MFP = \frac{\dot{m}}{A}\frac{\sqrt{T_t}}{P_t} = \sqrt{\frac{\gamma g_c}{R}M}\left(1 + \frac{\gamma - 1}{2}M^2\right)^{\frac{1+\gamma}{2(1-\gamma)}} \tag{3}$$

The hydraulic diameter can then be utilized to find the area at this station. Substituting the mass flow parameter into Equation 4, in combination with the area, total pressure and total temperature at this station, the mass flow rate aft of the turbine can be calculated.

$$\dot{m} = \frac{P_t g_c}{\sqrt{T_t}} A * MFP \tag{4}$$

The mass flow rate through the compressor core is given by the mass flow rate at the turbine exit minus the mass flow rate of the fuel, converted from pounds per hour to pounds per second. In order to isolate the performance of the compressor, the data must be reduced such that the affects of atmospheric temperature and pressure are normalized. This is accomplished by non-dimensionalizing the data, as shown in the following equations. Corrected mass flow rate is given by Equation 8.

$$\delta_t = \frac{P_t}{P_{ref}} \tag{5}$$

$$\theta_t = \frac{T_t}{T_{ref}} \tag{6}$$

$$N = \frac{RPM}{\sqrt{\theta_t}} \tag{7}$$

$$\dot{m}_c = \frac{\dot{m}\sqrt{\theta_t}}{\delta_t} \tag{8}$$

The pressure ratio for the compressor is simply given by Equation 9.

$$P_{ratio} = \frac{P_{t_3}}{P_{t_2}} \tag{9}$$

Utilizing Equations 7 through 9, the compressor map was generated by equally distributing an array of RPM values across the operating range of the collected data.

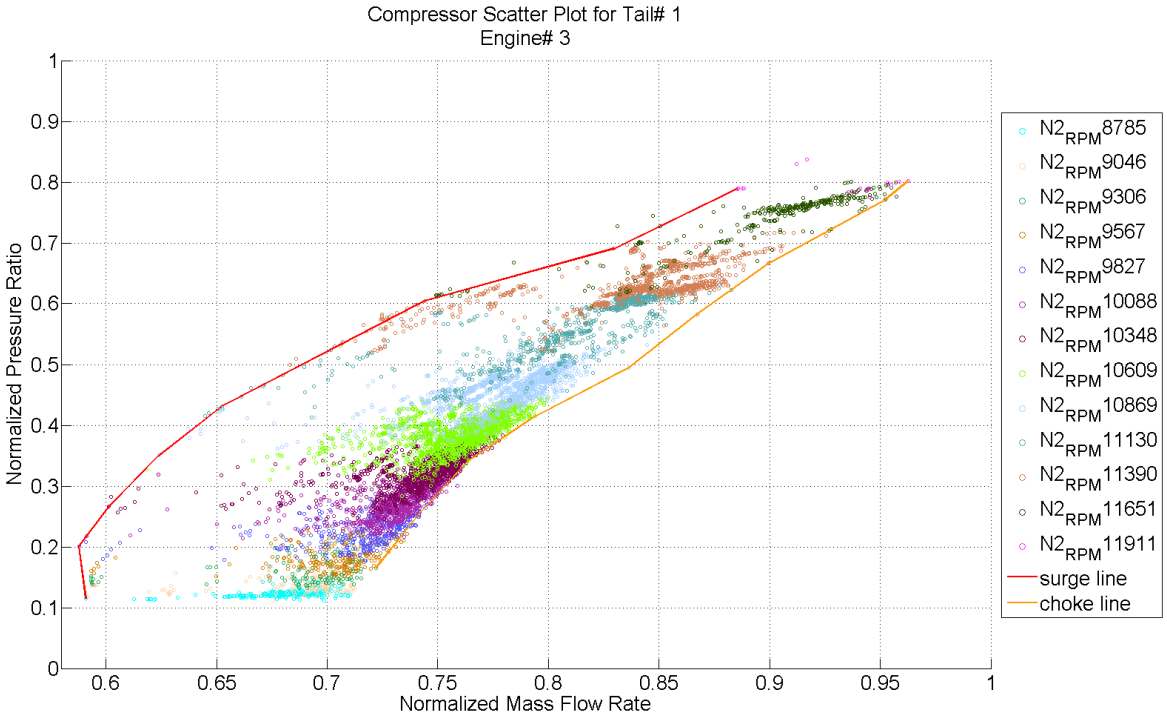

Figure 2: Scatter plot of corrected data organized by RPM groups.

Non-linear Regression and Linear Basis Expansion

Following the notation in Hastie,[5] et al. (2008), let $X \in \mathcal{R}^p$ denote a real valued random input vector (mass flow rate) and $Y \in \mathcal{R}$ a real valued random output variable (i.e., pressure ratio), with joint distribution $\Pr(X, Y)$. We seek a function $f(X)$ for predicting Y given values of the input X. Based on a loss function L(X,f(X)) for penalizing errors in prediction,

$$L\big(Y, f(X)\big) = (Y - f(X))^2$$

we would like to find the function that minimizes the expected prediction error (EPE) defined as $EPE(f) = EL\big(Y, f(X)\big)$. For squared error loss, it is easy to see that

$$\begin{aligned} EPE(f) &= EL\big(Y, f(X)\big) \\ &= E(Y - f(X))^2 \\ &= \int [y - f(x)]^2 \Pr(dx, dy) \\ &= E_X E_{Y|X}([Y - f(X)]^2 | X) \end{aligned}$$

For fixed values of X, we have

$$EPE(f) = E_{Y|X}([Y - f(X)]^2 | X)$$

And we see that the EPE is minimized, for each x, at

$$f(x) = E(Y|X = x).$$

Note that f(x) is known as the regression function and can be linear or non-linear. If the function is non-linear, we may still be able to estimate it using a linear expression through linear basis expansion functions. In this approach, we expand the design space using linear basis expansion, such as is done in polynomial regression. Denote $h_{jm}(\boldsymbol{X}) : \mathbb{R}^p \rightarrow \mathbb{R}$ by the mth transformation of $\boldsymbol{X}$, $m = 1, \ldots,$ M. We model

$$f(\boldsymbol{X}) = \sum_{j=1}^{p} f_j(X_j) = \sum_{j=1}^{p} \sum_{m=1}^{M_j} \beta_{jm} h_{jm}\big(X_j\big),$$

which represents linear basis functions in X. Note that the expression is linear in the parameters, $\beta_{jm}, m = 1, \ldots, M_j \; and \; j = 1, \ldots, p$. Some examples are

a. $h_m(X) = X_m, m = 1, \ldots, p$, which is the basis for multiple linear regression.
b. $h_m(X) = X_j^2 \; or \; h_m(X) = X_j X_k$, which allows for a higher-order Taylor expansion and represents the basis for quadratic response surface regression models.
c. $h_m(X) = X_1^{i_1} X_2^{i_2} \ldots X_p^{i_p}, i_j = 0,1, j = 1, \ldots, p$, which allows for higher-order polynomials and interactions. If we let, $h_1(X) = X_j, j = 1,2, \ldots, p, h_2(X) = X_j\, X_j, i < j\,, h_2(X) = X_i\, X_j X_k, i < j < k, \ldots, h_p(x) = X_1 X_2 \ldots X_p$, we will have $2^p - 1$ terms generated. In the case of p=3, we have, if we include an intercept term,

$$f(x) = \beta_0 + \beta_1 x_1 + \beta_2 x_2 + \beta_3 X_3 + \beta_4 x_1 x_2 + \beta_5 x_1 x_3 + \beta_6 x_2 x_3 + \beta_7 x_1 x_2 x_3$$

In this paper, we follow the above regression approach using the Bernstein polynomials as the basis expansion functions. These are described below.

The data was then grouped by RPM and a curve was fit to each RPM group. A number of different fits were explored in order to generate the best response for the data and included a linear fit, a least-squares polynomial fit and a Bernstein polynomial fit. To preserve the characteristics of the compressor operations while allowing for a dynamic fit to the data, a Bernstein polynomial was selected. This approach allows the function to remain fixed at the predicted surge and choke lines while allowing the shaping characteristics of the polynomial to accurately represent the intermediate operating conditions to the order *n*. The Bernstein polynomial typically defined over the interval 0-1 has been scaled to operate on a continuous function over the interval *a* to *b*, which is a function of the particular RPM being evaluated. For the Bernstein polynomials defined in Equation 10 by

$$B_{i,n}(t) = \frac{n!}{i!(n-i)!} t^i (1-t)^{n-i} \qquad (10)$$

there are *n*+1 *n*th-degree Bernstein polynomials, each term of which can be most easily represented by the Pascal triangle shown in Figure 3.

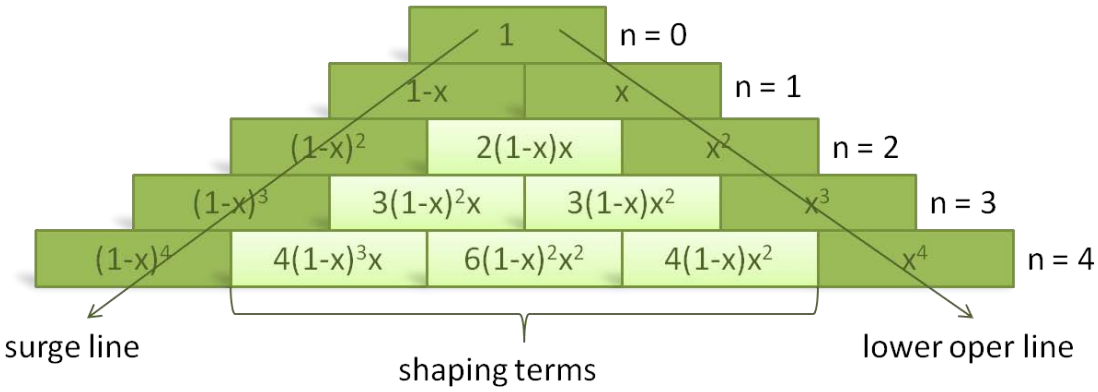

Figure 3: Pascal triangle of individual Bernstein polynomial terms up to n=4.

Before the Bernstein polynomials could be applied to the data set it was first necessary to define a series of control points. The control points for a number of speed lines are

represented by the vertices of the linear spline can be seen in Figure 4 and Figure 5.

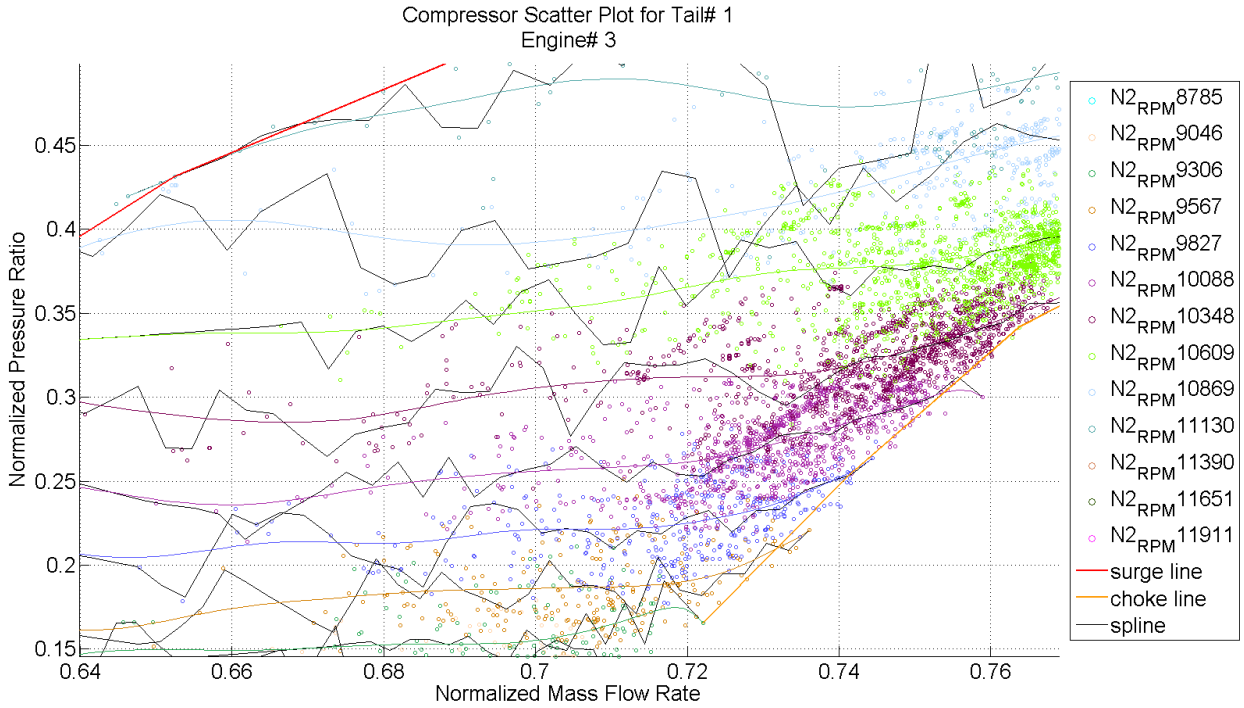

Figure 4: Control points and resulting speed line curves.

The control points were found by dividing each speed line into equally spaced segments and are shown by the pink and dark blue points in Figure 5. This data is further refined by selecting only the 25% which most closely match the RPM being analyzed. These data points are further separated into lower and upper values, pink and dark blue respectively, from which a lower and upper value is computed as the mean of their respective data points, depicted by the red in Figure 5. Finally the control point is linearly interpolated from the resultant upper and lower values for the given interval.

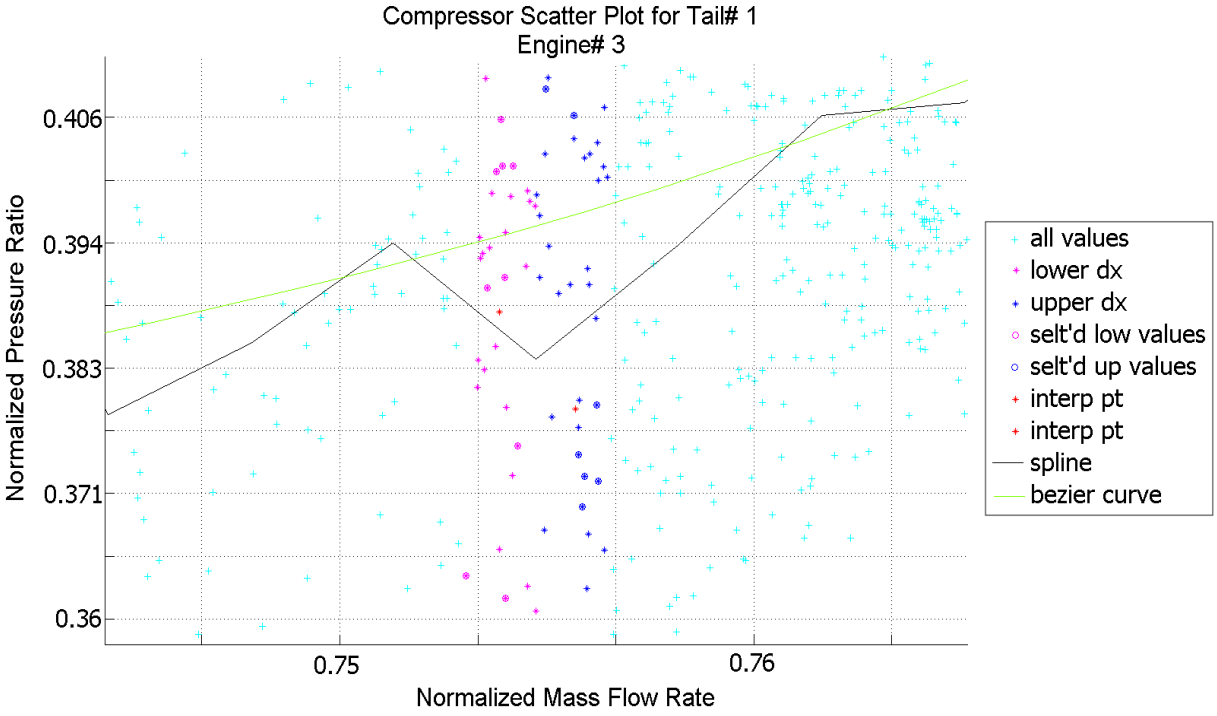

Figure 5: RPM segment for the computation of a single control point.

The complete set of control points, P_i, for each speed line is used to compute the Bezier Curve, *P(t)*, using Equation 11.

$$P(t) = \sum_{i=0}^{n} P_i B_{i,n}(t) \qquad (11)$$

The complete set of control points and the resulting curves can be seen in Figure 4 and the complete compressor map is shown in Figure 6.

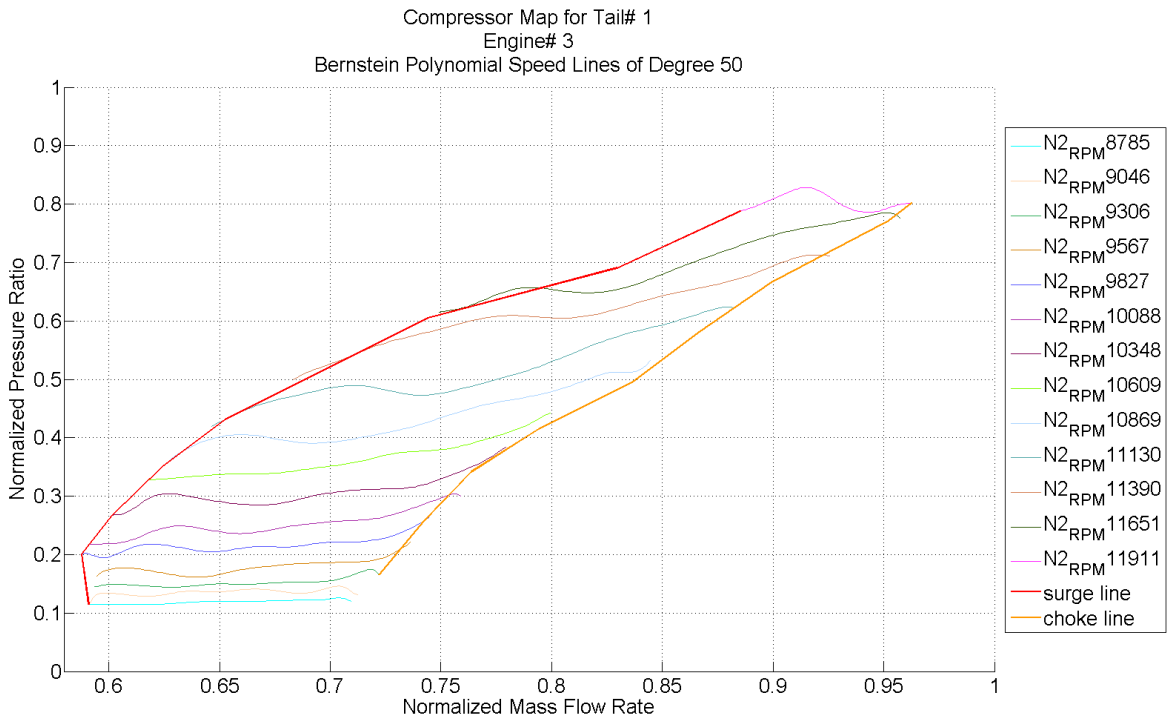

Figure 6: Single engine complete compressor map.

The Bernstein polynomial curves along with the normalized data from Equations 7, 8 and 9 were then further utilized to interpolate between RPM groups using a cubic spline and build a complete response surface for the compressor.

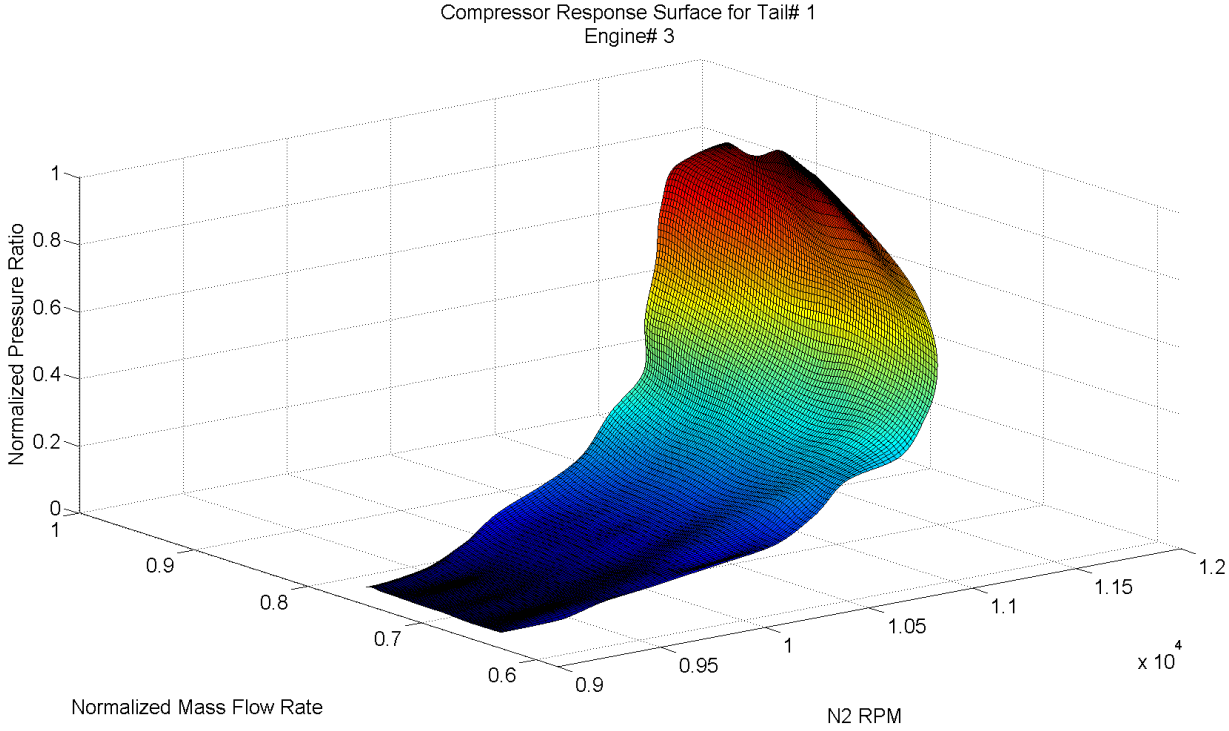

Figure 7: Single engine complete response surface.

Results and Discussion

The operating data from the engines of a single aircraft were processed as discussed above and the results are summarized in the following figures. In Figure 8, a number of the features of a compressor map become evident as the corrected values are plotted. First, the speed lines begin to appear as the various colors representing different RPMs group together and emerge from the data set. Second, overall performance of the compressor and engine are easily discernable. Third, a line connecting the data points along the far left hand side of the graph approximates the surge line for the compressor. Operations above the surge line result in a mass flow rate which is insufficient to maintain the given pressure ratio. The bleed valves at stages 5, 14 and 17, along with the variable IGVs and stators within the engine, are used to relieve the pressure and prevent cavitations which result in sudden loss of thrust and possibly even engine damage. Fourth, a line connecting the data points along the far right hand side of the graph approximates the choke line where the compressor is reaching its mass flow limit.

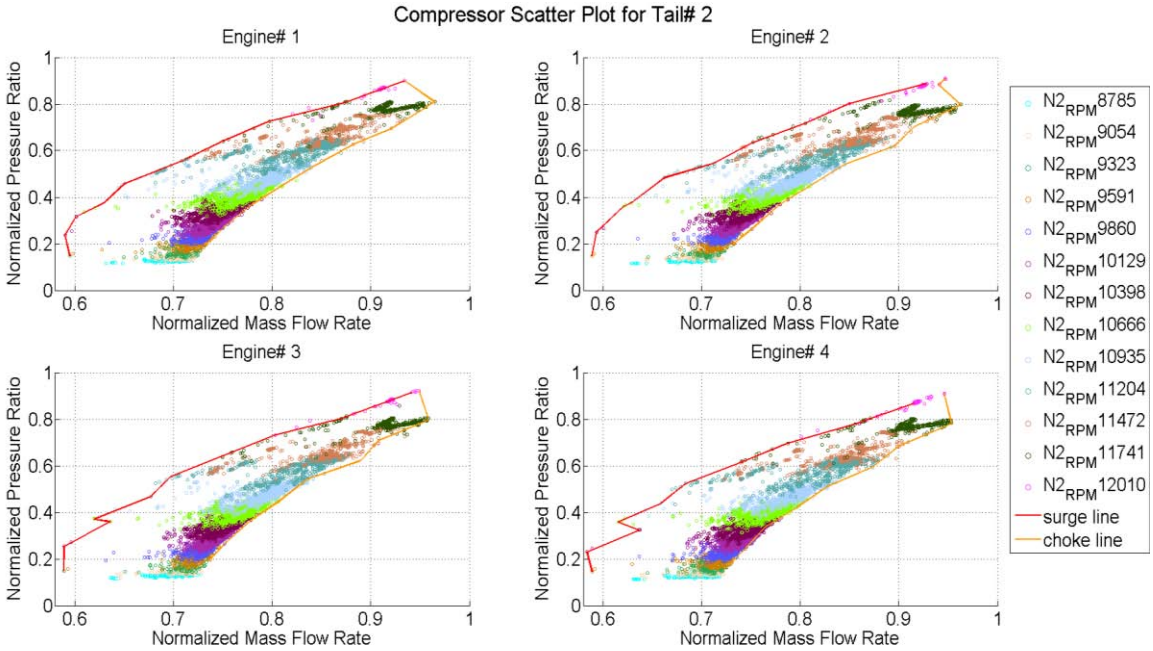

Figure 8: Compressor map scatter plots with RPM grouping, approx surge and choke lines for installed engines.

Figure 8 shows a large variance of pressure ratio and mass flow rate for each depicted interval of HPC RPM. This is most likely a result of the numerous different configurations the compressor bleed valves and stator angles can have, giving rise to differing flow parameters. In order to account for these variations and develop a more accurate parametric model of the compressor operations, further data pertaining to bleed

settings is required. Figure 9 depicts each speed line showing a good approximation of the operating conditions due to the endpoints being constrained by the surge and choke lines and the shaping terms of the Bernstein polynomial fitting the values in between.

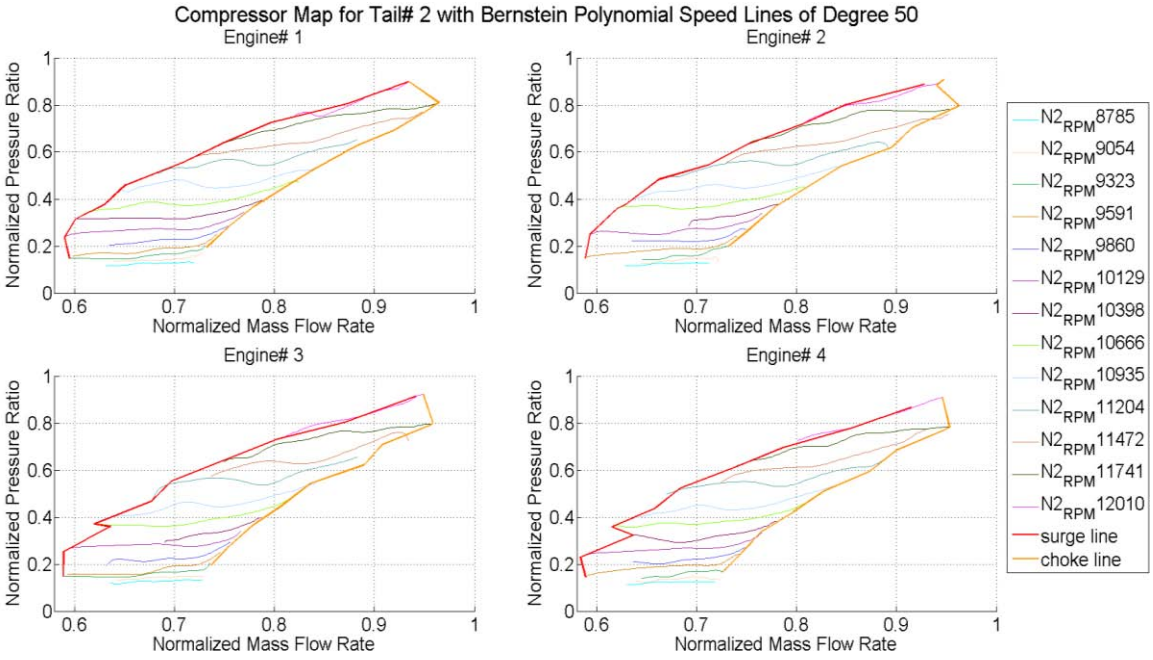

Figure 9: Speed lines fit using a Bernstein polynomial for installed engines.

Bernstein polynomials were applied to the speed lines and a complete response surface has been generated. The results can be seen in Figure 10. The response surface provides an analytical method to compute pressure ratio, given any combination of HPC RPM and mass flow rate. The response surface has been validated by calculating the coefficient of determination (R^2). The residual for each of the points has been calculated and the resulting sum of squares of residual (SSE) along with the total sum of squares (SST) and R^2. The results for each surface are tabulated versus the data from its own and the accompanying three engines from the aircraft in Table 1. Furthermore, a visual representation of the goodness-of-fit is provided by Figure 11, which gives two different perspectives of the response surface overlaid with the captured data points for its own engine. Both the graphical depiction and the calculated values for the goodness-of-fit suggest this is a well behaved model which accounts for almost 99% of the variance in pressure ratio capable of accurately modeling performance of this family of engines operating under a given set of conditions.

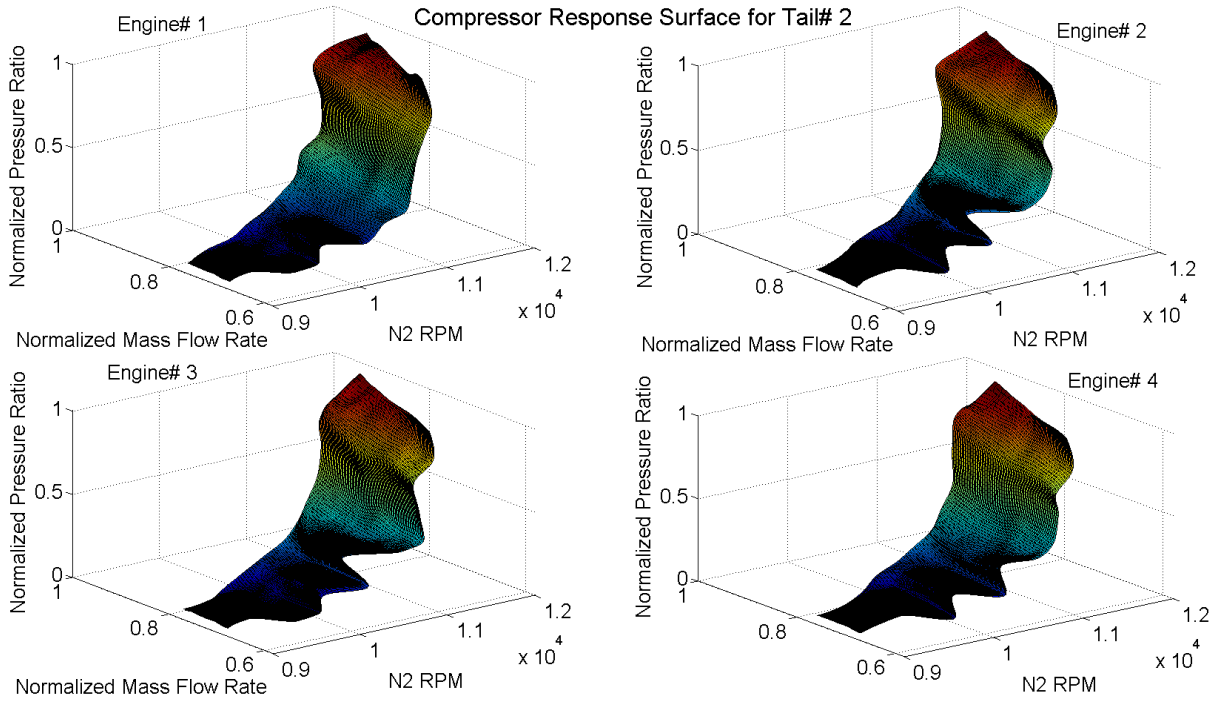

Figure 10: Compressor with Bernstein polynomial response surface, installed engines.

Table 1: Goodness-of-fit results for each response surface vs. each engines' data capture.

	E1 Surface	E2 Surface	E3 Surface	E4 Surface
E1 Data	0.9893	0.9878	0.9884	0.9858
E2 Data	0.9892	0.9899	0.9893	0.9889
E3 Data	0.9893	0.9889	0.9896	0.9875
E4 Data	0.989	0.9897	0.9893	0.9905

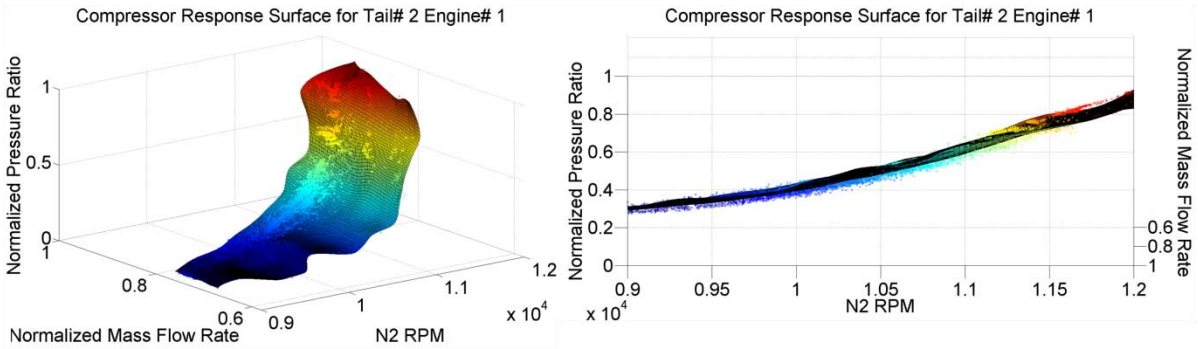

Figure 11: Response surface and captured data overlay.

Further performance analysis is conducted by comparing the response surfaces of each engine against each other engine on an aircraft. For this analysis, a jet with engines of significantly different operating life times is selected. Figure 12 shows the margin plots for this aircraft and clearly shows engine #2 having a much lower margin, approximately -3°C, than any other engine on this aircraft.

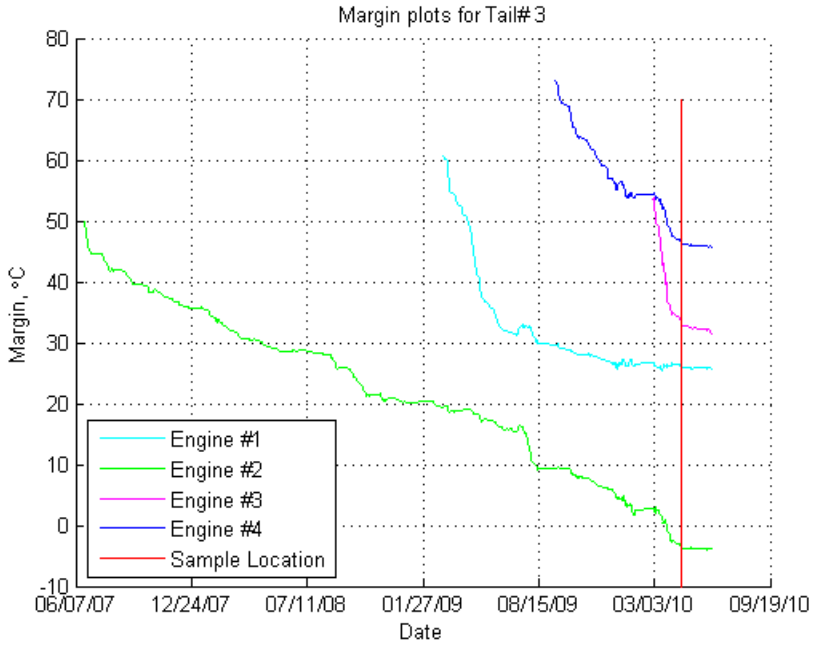

Figure 12: Engine operating temperature margin as a function of time.

When each point on the response surface is subtracted from the matching point on each of the other response surfaces, the following figures are generated. An overhead perspective of the resulting plots clearly illustrates portions of the operating regime where compressor ratios are higher or lower than the comparative engine. Figure 14 is of particular interest as it shows the results of a low margin engine. Here, it can be seen that the compressor is operating with higher pressure ratios under most conditions and, in

particular, along the surge line when compared to the others as a result of its increased operating demands in order to produce the same exit pressure ratio as the other engines.

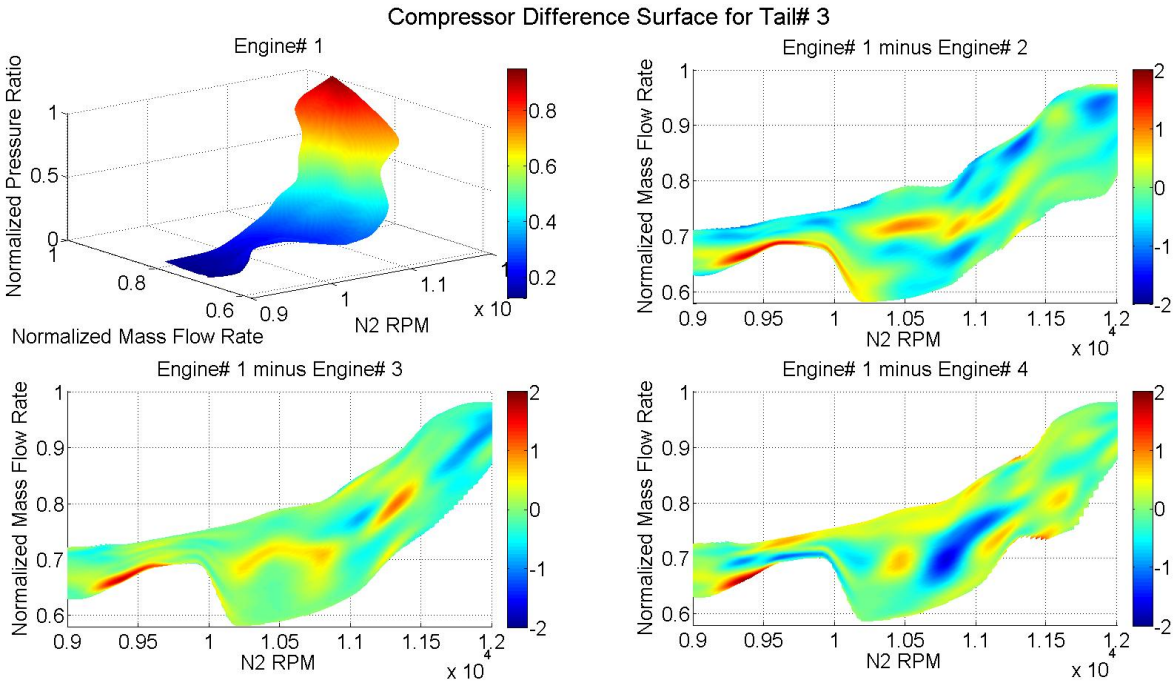

Figure 13 Engine #1 compressor performance.

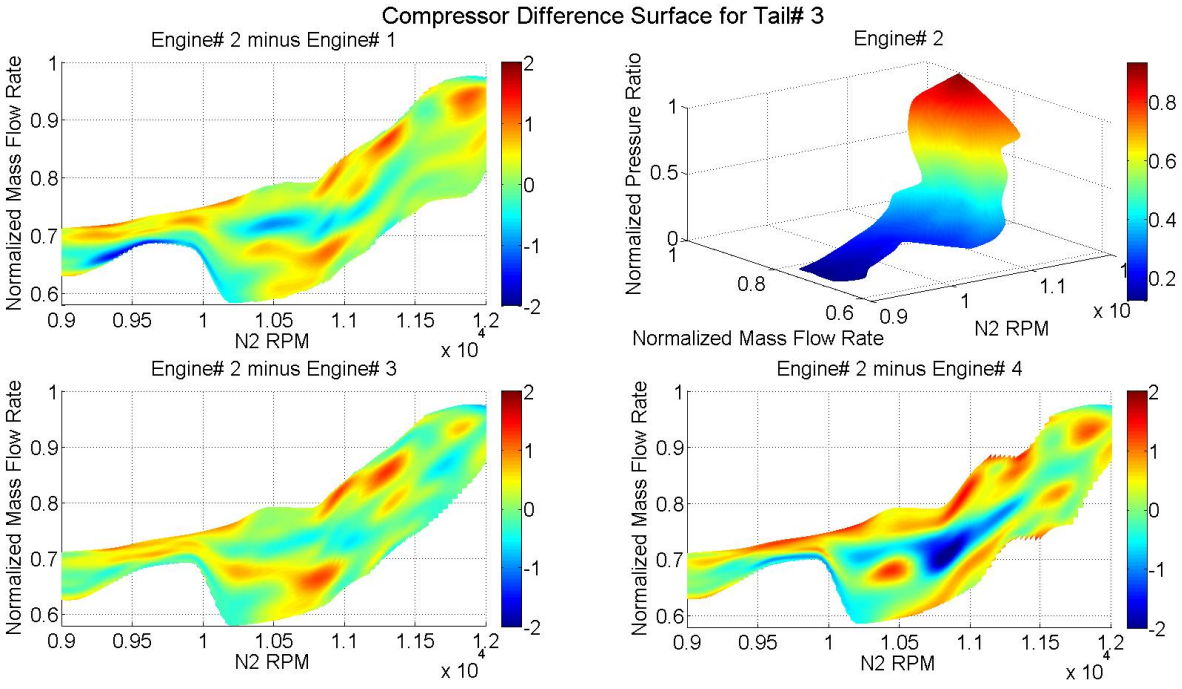

Figure 14: Engine #2 compressor performance.

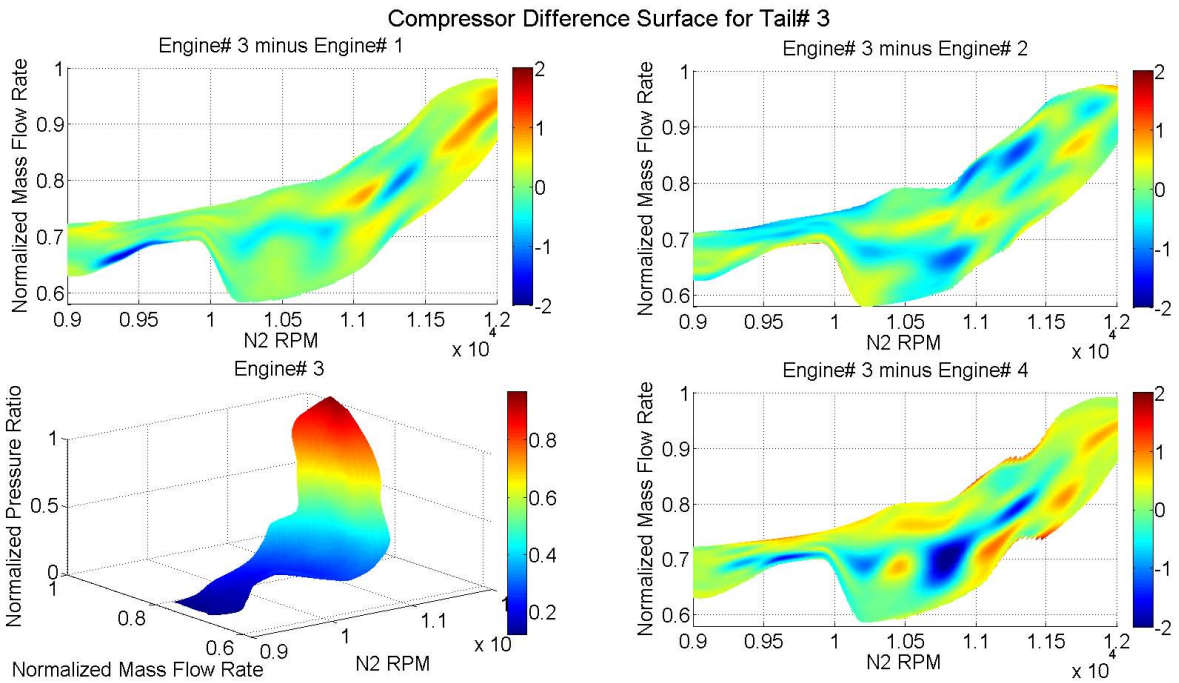

Figure 15 Engine #3 compressor performance.

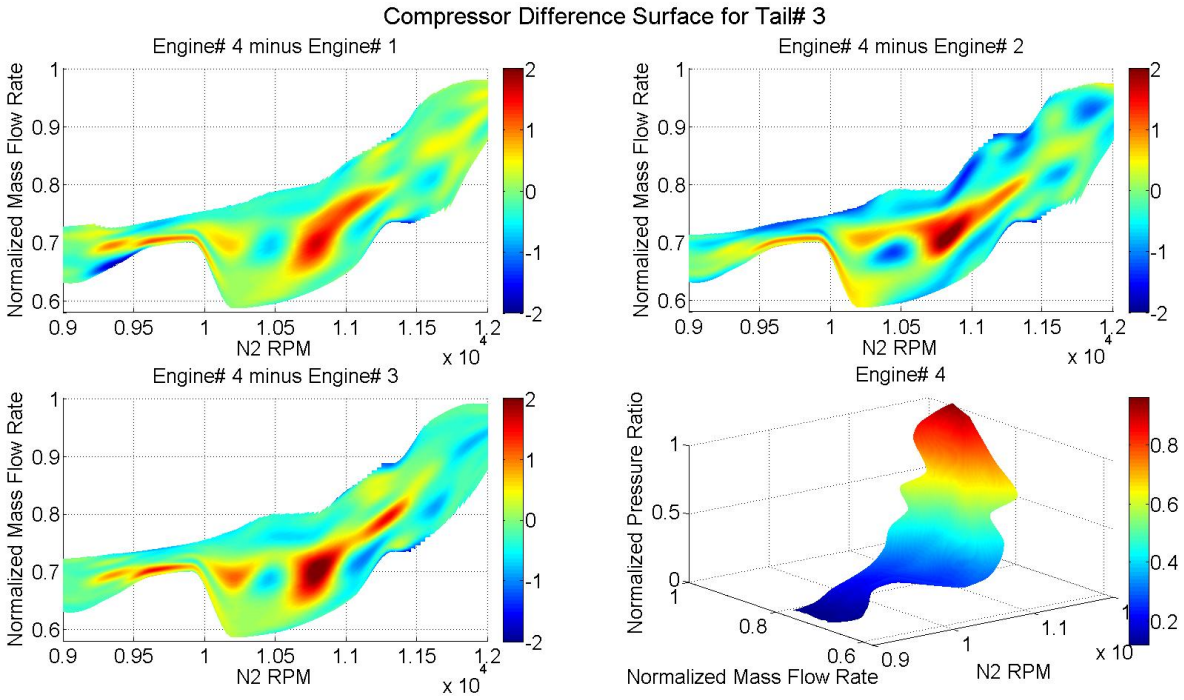

Figure 16 Engine #4 compressor performance.

Conclusion

Data from a modern compressor has been captured from a wide range of missions and operating conditions, providing a complete platform upon which to conduct an analysis. The data was first normalized to eliminate variation from atmospheric conditions, and then it was used to calculate the corrected mass flow rate and the overall pressure ratio of the compressor. The resultant data was further reduced to generate speed lines using a Bernstein polynomial approach and a compressor map was generated. The compressor map was then further developed to provide a complete response surface for the compressor. The surface provides a function by which pressure ratio can be derived from HPC RPM and compressor mass flow rate. The response surfaces provide the surge and choke lines of the compressor. The accuracy of the model has been determined by inspection of the data and calculation of the coefficient of determination which suggests that the model accounts for almost 99% of the variation in the response variable, pressure ratio. Further analysis of the response surface can be used to provide optimal and safe control and operation over the life of the engine.

References

1. Ghorbanian, K. and Gholamrezaei, M., "An artificial neural network approach to compressor performance prediction,"*Applied Energy* 86 (2009) 1210–1221.
2. Flack, R., *Fundamentals of Jet Propulsion with Applications,* Cambridge University Press, 2005.
3. Mattingly, Jack D., *Elements of Propulsion: Gas Turbines and Rockets,2nd Ed.*, AIAA, Reston, Virginia, 2006
4. Mathew, J. and Fink, K., *Numerical Methods Using MATLAB 4th Ed*, Prentice-Hall Inc., Upper Saddle River, New Jersey, 2004
5. Hastie, Trevor, Tibshirani, Robert, and Friedman, Jerome (2008), The Elements of Statistical Learning: Data Mining, Inference, and Prediction, Second Edition, Springer-Verlag